Phytochemistry 171 (2020) 112233

Contents lists available at ScienceDirect

Phytochemistry

journal homepage: www.elsevier.com/locate/phytochem

Bioactive chemical constituents from the seed testa of *Vernicia fordii* as potential neuroinflammatory inhibitors

Gang Chen[a,e,1], Weihong Zhao[a,e,1], Yang Li[a,e], Di Zhou[a,e], Jing Ding[a,e], Bin Lin[c], Wei Li[a,e,b], Yanqiu Yang[d,e], Jingyu Liu[d,e], Yue Hou[d,e,*], Ning Li[a,e,**]

[a] School of Traditional Chinese Materia Medica, Shenyang Pharmaceutical University, Shenyang, 110016, PR China
[b] Faculty of Pharmaceutical Sciences, Toho University, Miyama 2-2-1, Funabashi, Chiba, 274-8510, Japan
[c] School of Pharmaceutical Engineering, Shenyang Pharmaceutical University, Shenyang, 110016, PR China
[d] College of Life and Health Sciences, Northeastern University, Shenyang, 110004, China
[e] State Key Laboratory for Chemistry and Molecular Engineering of Medicinal Resources, Guangxi Normal University, Guilin, China

ARTICLE INFO

Keywords:
Euphorbiaceae
Vernicia fordii
Phenylpropanoids
Anti-neuroinflammatory effects
Neurodegenerative diseases

ABSTRACT

Eight previously undescribed and 15 known components, including six neolignans, two monolignan, three sesquineolignans, three dineolignans, eight phenylpropanoids, and one steroid were identified from the seed testa of *Vernicia fordii*. Their structures were established based on the comprehensive analysis of NMR and ECD data. The anti-neuroinflammatory effects of the isolates were evaluated through nitrite assays in LPS-induced BV2 cells. As a result, isodiverniciasin A, diverniciasin B, diverniciasin C, isoprincepin, princepin, 3, 3′-bisdemethylpinoresinol, (+)-7-epi-sesamin-dicatechol, isoamericanin A, americanin B, 7*S*, 8*R*-americanin D, 4-hydroxyl cinnamic aldehyde, 3-hydroxyl-4-methoxyl cinnamic aldehyde and 24*R*-6*β*-hydroxy-24- ethylcholest-4-en-3-one exhibited significant inhibitory effects on nitric oxide (NO) production and isoprincepin, princepin, americanin B, and 4-hydroxyl cinnamic aldehyde suppressed the overexpression of inflammatory cytokines TNF-α, IL-1β, and IL-6 in over-activated microglia. The results suggested that bioactive ingredients from the seed testa of *V. fordii* can serve as potential therapeutic agents for neurodegenerative diseases.

1. Introduction

Vernicia fordii (Hemsl.) Airy Shaw (Euphorbiaceae), usually known in China as the tung tree, is mainly distributed in the east of Asia, and its seeds, roots, flowers, and leaves have been used in folk medicine for generations. Previous studies have revealed that its seed oil can treat burn, scald, and cold injuries (Ran, 2009; Liao, 2009; Zhang, 2003; Guo et al., 2002). The crude extract of leaves of *V. fordii* have also been reported to possess anti-bacteria activities. However, very few papers have reported its chemical constituents. A toxic diterpenoid diester 12-*O*-palmityl-13-*O*-acetyl-16-hydroxyphorbol and a monoester 13-*O*-acetyl-16-hydroxyphorbol were isolated from its fruits (Okuda et al., 1975), and piscidal constituents and related diterpene esters have been identified from the leaves (Hirota et al., 1979). Moreover, triterpenes from its leaves exhibit significant growth-inhibitory effects on human cancer cells (Pei et al., 2013). From its roots, one phorbol diester 12-*O*-palmityl-13-*O*-acetyl-16-hydroxyphorbal, one coumarinolignoid aleuritin, and other constituents including (−) syringaresinol, daucosterol, 4-hydroxy-3, 5-dimethoxybenzolic acid, and acetyl aleuritolic acid were isolated. (Xie et al., 2010). From the seeds, lupinane type triterpenes and flavonoids have been detected (Mao et al., 2012). Therefore, further investigations regarding the chemical constituents and pharmacological activities of *V. fordii* are needed to explore its potential pharmaceutical applications.

In our continuous studies on natural neuroinflammatory inhibitors, the testa of *V. fordii* attracted our interest because of its remarkable inhibitory effect on nitric oxide (NO) production in over-activated microglia cells. The excessive stimulation of microglia results in the production of pro-inflammation cytokines and cytotoxic substances, such as tumor necrosis factor (TNF-α) and NO. These secretions, in turn, stimulate the activated microglia cells, leading to neuroinflammation involved in neurodegenerative diseases, including Alzheimer's and Parkinson's disease. Therefore, the potent inhibitory effect on NO production of *V. fordii* suggested its great potential for use in treating of

* Corresponding author. School of Traditional Chinese Materia Medica, Shenyang Pharmaceutical University, Wenhua Road 103, Shenyang, 110016, China.
** Corresponding author. College of Life and Health Sciences, Northeastern University, Shenyang, 110004, China.
E-mail addresses: liningsypharm@163.com (Y. Hou), houyue@mail.neu.edu.cn (N. Li).
[1] Gang Chen and Weihong Zhao contributed equally to this article.

https://doi.org/10.1016/j.phytochem.2019.112233
Received 31 May 2019; Received in revised form 7 December 2019; Accepted 18 December 2019

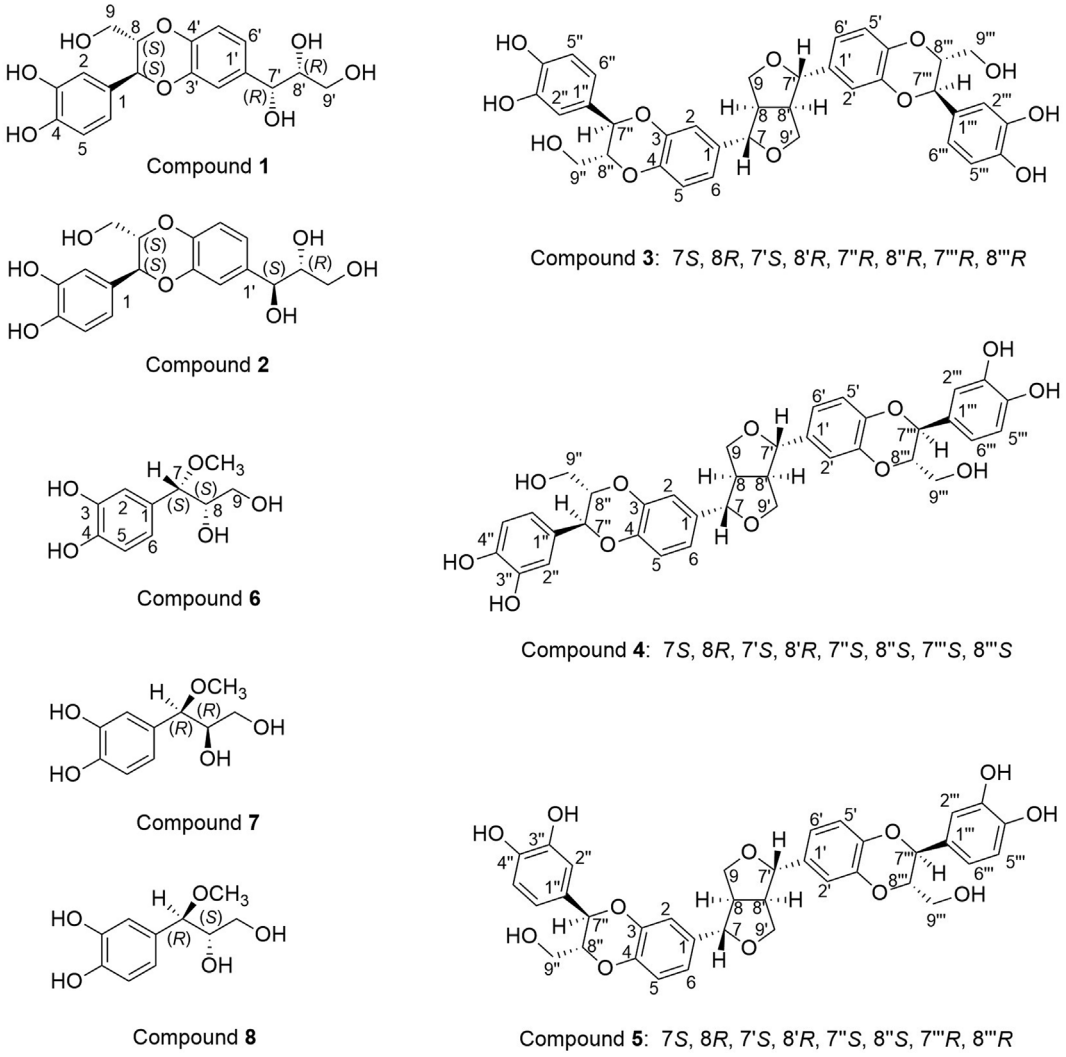

Fig. 1. The structures of undescribed lignans **1–8.**

neurodegenerative diseases. Further studies have indicated that the ethyl acetate extract of the seed testa of *V. fordii* is responsible for the anti-neuroinflammatory effects. Therefore, bioactivity-guided phytochemical research was carried out to clarify the effective material basis. In this study, the isolation, structural identification, and *in vitro* anti-neuroinflammatory activities of eight previously undescribed and 15 known isolates from the ethyl acetate extract of the seed testa of *V. fordii* are reported.

2. Results and discussion

2.1. Identification of the undescribed lignans

The present study mainly describes the separation, elucidation, possible biosynthesis pathways, and *in vitro* anti-inflammatory activities of the constituents isolated from the bioactive extract of the seed testa of *V. fordii.* As a result, **23** compounds (Figs. 1 and 2) were characterized through extensive NMR spectra analysis. Among them, to the best of our knowledge, compounds **1–8** (Fig. 1) have not been described before and compounds **9–10** and **13–21** were obtained from this genus for the first time.

Compound **1** was obtained as a light-yellow syrup. [α] 20D -13.6 (*c* 0.15, MeOH). Its negative HRESI-MS spectra suggested the molecular formula $C_{18}H_{20}O_8$ by the m/z 363.1083 $[M\text{-}H]^-$ (calcd. 363.1080 for $C_{18}H_{19}O_8$). ^{1}H NMR data (see Table 1) indicated the presence of two 1,3,4 - trisubstituted aromatic groups that resonated at δ_H 6.84 (1H, d, J = 1.1 Hz, H-2′), δ_H 6.82 (1H, d, J = 8.0 Hz, H-5′), 6.79 (1H, dd, J = 8.0, 1.1 Hz, H-6′), 6.80 (1H, d, J = 1.4 Hz, H-2), 6.75 (1H, d, J = 8.0 Hz, H-5) and 6.69 (1H, dd, J = 8.0, 1.4 Hz, H-6). The ^{13}C NMR spectra revealed 18 carbon signals assigned to 12 aromatic carbons, four methines (δ_C 78.2, 75.6, 75.2, 73.5) and two methylenes (δc 60.2, 63.1). In addition to the HMBC correlations of H-9/C-8, C-7; H-8/C-7, C-1; H-9'/C-8′, C-7'; H-8'/C-7′, C-1' (Fig. 3), two C6–C3 fragments were deduced (C-1 to C-9; C-1′ to C-9′ as shown in Fig. 1), suggesting that **1** was a neolignan. Subsequently, HMBC correlations of H-7/C-3′ and H-8/C-4' (Fig. 3) determined the linkage of two C6–C3 units and thereby established the structure of **1** named as verniciasin B (Fig. 1).

The relative configuration of C-7/C-8 was revealed by the coupling constant of H-7 [δ_H 4.78 (1H, d, J = 7.8 Hz)], suggesting a trans configuration of C-7/C-8 (Kim et al., 2010). Meanwhile, the coupling constant of H-7' [δ_H 4.33 (1H, d, J = 6.0 Hz)] suggested a *threo* configuration for the hydroxyl groups at C-7′ and C-8' (Kim et al., 2013), which was further verified by the empirical rule of chemical shifts at C-7′ and C-8' ($\triangle\delta_{|7'\text{-}8'|} < 2$) (Gan et al., 2008). Therefore, the absolute configuration of C-7′ and C-8′ were indicated as 7′*S*,8′*S* or 7′*R*,8′*R*. The absolute configurations of C-7 and C-8 were determined using the CD exciton chirality method (Adam et al., 2000), through which a positive chirality for 7*S*, 8*S* isomer of **1** was proposed by the observed clockwise rotation of the two excitons (Fig. 4A). In the experimental CD spectra of **1**, a positive cotton effect from long wavelength (225 nm) and a

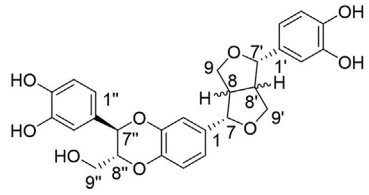

Compound **9** isoprincepin

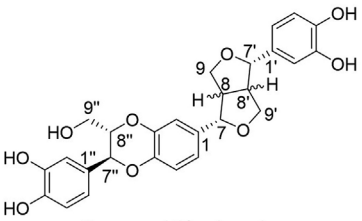

Compound **10** princepin

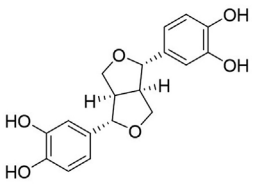

Compound **11** (±)-3,3'-bisdemethylpinoresinol

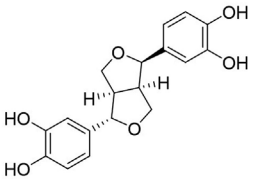

Compound **12** (+)-7-epi-sesamin-dicatechol

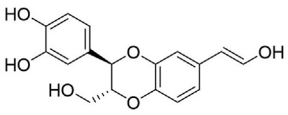

Compound **13** isoamericanol A

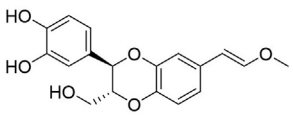

Compound **14** 9'-methoxylisoamericanol A

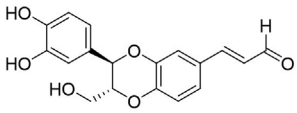

Compound **15** isoamericanin A

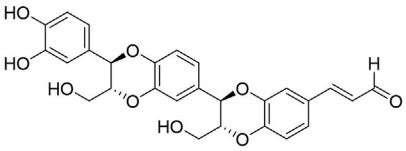

Compound **16** americanin B

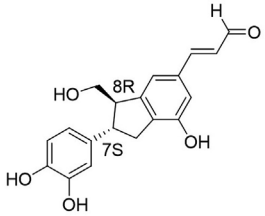

Compound **17** 7S,8R-americanin D

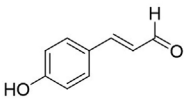

Compound **18**

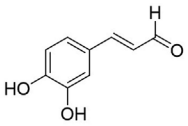

Compound **19**

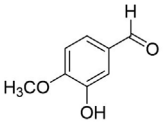

Compound **20**

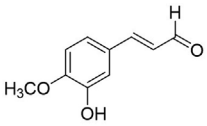

Compound **21**

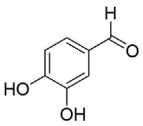

Compound **22**

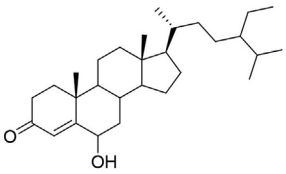

Compound **23**

Fig. 2. The structures of **9**–**23.**

negative one around 200 nm were observed, indicating the absolute configurations of **1** were 7*S* and 8*S*. The absolute configurations of C-7(*S*) and C-8(*R*) proposed by the CD exciton chirality method were further confirmed through an ECD simulation using DFT calculation. As shown in Fig. 4B, the calculated ECD spectra of the 7*S*, 8*S* isomer perfectly matched the experimental ECD curves of **1** at 225 and 200 nm (Fig. 4B). Moreover, the calculated ECD curves of the 7*S*, 8*S,* 7′*R*, 8′*R*-isomer perfectly aligned with those of the experimental ECD curves at both 200–225 and 230 nm (Fig. 4B). Therefore, the structure of **1** was finally determined as 7*S*, 8*S,* 7′*R*, 8′*R* -verniciasin B.

Compound **2** was obtained as a yellow syrup with [α] 20D-35.9 (*c* 0.15, MeOH), having the same molecular formula as **1** due to the quasi-molecular ion peak *m/z* 363.1085 [M-H]$^-$ (calcd. 363.1085 for $C_{18}H_{19}O_8$) observed in the negative HRESIMS spectra. HMBC correlations of **2** (Fig. 3) and the extensive comparison of the ^{1}H NMR and ^{13}C NMR data of **2** with those of **1** (see Table 1) suggested that they possessed the same planar structure. The main difference observed for **2** was presented at the chemical shift of C-7' (δ_C 72.4 in compound **2** and δ_C 73.5 in compound **1**) and C-8' (δ_C 75.8 in compound **2** and δ_C 75.2 in compound **1**), indicating a C-7′/8′ *erythro* (Kim et al., 2013) configuration (7′*S*,8′*R* or 7′*R*,8′*S*). The consistent result was obtained by the empirical rule of chemical shifts at C-7′ and C-8' ($\triangle\delta_{|7'\text{-}8'|} > 2$) in compound **2** (Gan et al., 2008). The calculated ECD spectra of the 7*S*, 8*S,7′S*,8′*R*-isomer perfectly matched that of the experimental ECD spectra of **2** (Fig. 4C). Therefore, compound **2** was identified as 7*S*, 8*S,7′S*,8′*R*-verniciasin B.

Compound **3** was separated as a colorless amorphous solid with [α] 20D -10.0 (*c* 0.1, MeOH). Its molecular formula was determined to be $C_{36}H_{34}O_{12}$ by the quasi-molecular ion peak m/z 681.1942 [M+Na]$^+$ (calcd. 681.1940 for $C_{36}H_{34}NaO_{12}$) in the positive HRESIMS spectra. The ^{1}H NMR spectra afforded the presence of two ABX coupling systems with resonances at δ_H 6.87 (2H, br. s, H-2, 2′), 6.88 (2H, d, *J* = 8.3 Hz, H-5, 5′), 6.85 (2H, br. d, *J* = 8.3 Hz, H-6, 6′), 6.78 (2H, br. s, H-2″, 2‴), 6.74 (2H, d, *J* = 8.0 Hz, H-5″, 5‴) and δ_H 6.68 (2H, dd, *J* = 8.0, 0.8 Hz, H-6″, 6‴). The ^{13}C NMR spectra only revealed 18 carbon signals, suggesting a symmetrical structure in **3**. In the ^{13}C NMR spectra, 12 aromatic and six sp^3 signals were observed (Table 2), indicating the presence of two C6–C3 fragments in **3**. The ^{13}C NMR signals at δ_C 84.6,

Table 1
The ^{1}H-NMR (600 Hz) and^{13}C-NMR (150 Hz) data of compounds **1** and **2** (DMSO-d_6).

No.	Comp.**1**		Comp.**2**	
	δ_H	δ_C	δ_H	δ_C
1	–	127.8	–	127.8
2	6.80 (d, 1.4)	114.9	6.80 (br.s)	115.0
3	–	145.2	–	145.3
4	–	145.7	–	145.8
5	6.75 (d, 8.0)	115.5	6.79 (d, 8.0)	115.5
6	6.69 (dd, 8.0, 1.4)	118.8	6.69 (br.d, 7.8)	118.8
7	4.78 (d, 7.8)	75.6	4.79 (d, 7.6)	75.6
8	3.97 (m)	78.2	3.98 (m)	78.2
9	3.51 (m); 3.32 (m)	60.2	3.51 (m); 3.33 (m)	60.2
1′	–	136.4	–	136.4
2′	6.84 (d, 1.1)	115.5	6.83 (br.s)	115.8
3′	–	142.8	–	142.9
4′	–	141.9	–	142.0
5′	6.82 (d, 8.0)	115.5	6.84 (d, 8.0)	115.8
6′	6.79 (dd, 8.0, 1.1)	120.0	6.75 (br.d, 7.8)	119.4
7′	4.33 (d, 6.0)	73.5	4.41 (d, 2.9)	72.4
8′	3.51 (m)	75.2	3.51 (m)	75.8
9′	3.44 (m); 3.37 (m)	63.1	3.44 (m); 3.34 (m)	62.6

53.6, 71.0 identified a “furofuran ring system” (Reiner et al., 2003). In addition, the carbons at δ_C 75.7, 78.2, and 60.2 were the typical signals of a dioxane moiety. Combined with the aforementioned symmetrical feature, **3** was deduced as a dineolignan. HMBC correlations from H-7 to C-1, C-2, and C-6; from H-7″ to C-3, C-1″, C-2″, C-6″, C-8″, and C-9" (Fig. 2) linked the two ABX coupling systems. Therefore, the planner structure of **3** was determined as shown in Fig. 1 and was named as isodiverniciasin A.

The proton signal at δ_H 4.81 (2H, d, J = 7.7 Hz, H-7″) prompted that 7"/8″ was a *trans* configuration. The 7-H/8-H *trans* and 7′-H/8′-H *trans* configurations were determined due to the chemical shift differences of $\Delta\delta_{H\text{-}9}$ and $\Delta\delta_{H\text{-}9'}$ ($\Delta\delta$ = 0.36 ppm) (Shao et al., 2018). The relative configuration of the H-7 and H-7′ of the furofuran ring system was elucidated as a *cis* configuration by both the chemical shifts and the characteristic of symmetry compared with those of 3, 3′-bisdemethylpinoresinol (Kamiya et al., 2004). The NOSEY spectra of **3** revealed the NOE correlation of H-7/H-9, further substantiating the *cis* configuration H-7 and H-7' (Fig. 5). The absolute configurations of **3** were also determined via a ECD simulation using DFT calculation, and the calculated ECD spectra of the 7*S*, 8*R*, 7′*S*, 8′*R*, 7″*R*, 8″*R*, 7*R*, 8*R* -isomer of **3** showed almost identical ECD curves to those of the experimental ECD spectra (Fig. 4D). Therefore, compound **3** was elucidated as 7*S*, 8*R*, 7′*S*, 8′*R*, 7″*R*, 8″*R*, 7*R*, 8*R* - isodiverniciasin A.

Compound **4** was purified as a colorless solid with [α] 20D-61.0 (*c* 0.1, MeOH). Its molecular formula was determined to be $C_{36}H_{34}O_{12}$, which is the same as that of **3**, due to the quasi-molecular ion peak m/z 657.1974 [M-H]$^-$ (calcd. For 657.1978) in the negative HRESIMS spectra. The ^{13}C NMR spectra also afforded 18 carbon signals as **3**, suggesting that the structure of **4** was also symmetric. In addition, the ^{1}H NMR and ^{13}C NMR data (see Table 2) of **4** were almost identical to those of **3**, except for the proton resonances at δ_H 6.92 (2H, d, J = 1.3 Hz, H-2, 2′), 6.86 (2H, d, J = 8.3 Hz, H-5, 5′) and δ_H 6.83 (2H, dd, J = 8.3, 1.3 Hz, H-6, 6′), and the carbon chemical shifts at δ_C 143.0, 143.1 (C-3, 3′) and δ_C 142.9 (C-4, 4′). Through comparing the proton signals of **3** and **4**, a $\triangle\delta_H$ 0.01 ppm between H-2/2′ and H-5/5′ and a $\triangle\delta_H$ 0.03 ppm between H-2/2′ and H-6/6′ in ^{1}H NMR spectra of **3** were detected, while for **4** the $\triangle\delta_H$ were 0.06 and 0.09 ppm between H-2/2′ and H-5/5′ and between H-2, 2′ and H-6, 6′, respectively. These results suggest the existence of an isoamericanol type of structure in **3** and an americanol-type structure in compound **4** (Reiner et al., 2003). In HMBC spectra of **4**, the correlation from H-7"/7‴ (4.80) to C-4/4' (142.9) was observed, further proving the existence of americanol-type structures in compound **4**. Finally, in conjunction with further analysis on the HMBC data (Fig. 2), the planar structure of **4** was deduced as shown in Fig. 1, named as diverniciasin C.

The proton signal at δ_H 4.80 (2H, d, J = 7.7 Hz, H-7″) prompted that 7"/8″ was a *trans* configuration. The 7-H/8-H *trans* and 7′-H/8′-H *trans* configurations were also determined by the value of $\Delta\delta_{H\text{-}9}$ and $\Delta\delta_{H\text{-}9'}$ ($\Delta\delta$ = 0.36 ppm) (Shao et al., 2018). The relative configuration of the H-7 and H-7′ of the furofuran ring system was also elucidated as a *cis* configuration by the same methods used in the elucidation of **3** (Kamiya et al., 2004) (Fig. 4). The ECD calculation was adopted to determine the absolute configurations of **4**. As a result, the calculated ECD cotton effects of 7*S*, 8*R*, 7′*S*, 8′*R*, 7″*S*, 8″*S*, 7*S*, 8*S* -isomer were in good agreement with those of the experimental ECD spectra of **4** (Fig. 4E). Therefore, **4** was determined as 7*S*, 8*R*, 7′*S*, 8′*R*, 7″*S*, 8″*S*, 7*S*, 8*S* -diverniciasin C.

Diverniciasin B (**5**) was isolated as a colorless solid with [α] 20D-18.0 (*c* 0.1, MeOH). Its molecular formula was determined to be $C_{36}H_{34}O_{12}$ by the quasi-molecular ion peak m/z 657.1984 [M-H]$^-$ (calcd. 657.1978 for $C_{36}H_{34}O_{12}$) observed in the negative HRESIMS spectra. As opposed to **3** and **4** that only revealed 18 carbon signals, **5** gave 36 carbon signals, suggesting the absence of symmetric structures in **5**. Nonetheless, the NMR signals of **5** also resembled those of **3** and **4**, including four ABX coupling systems (Table 3). The difference of

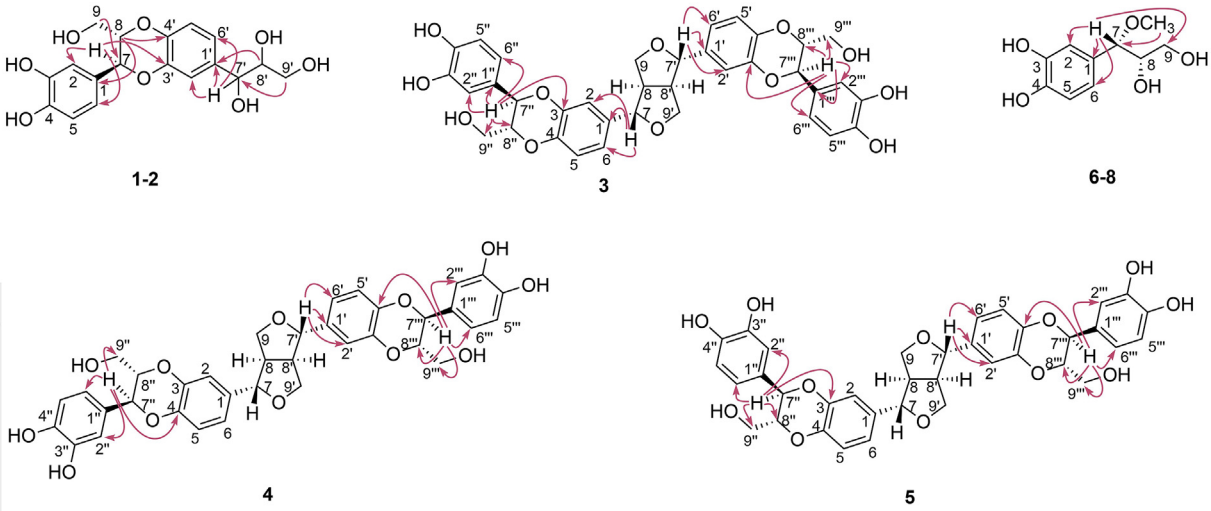

Fig. 3. The key HMBC correlations (↷) of compounds **1–8.**

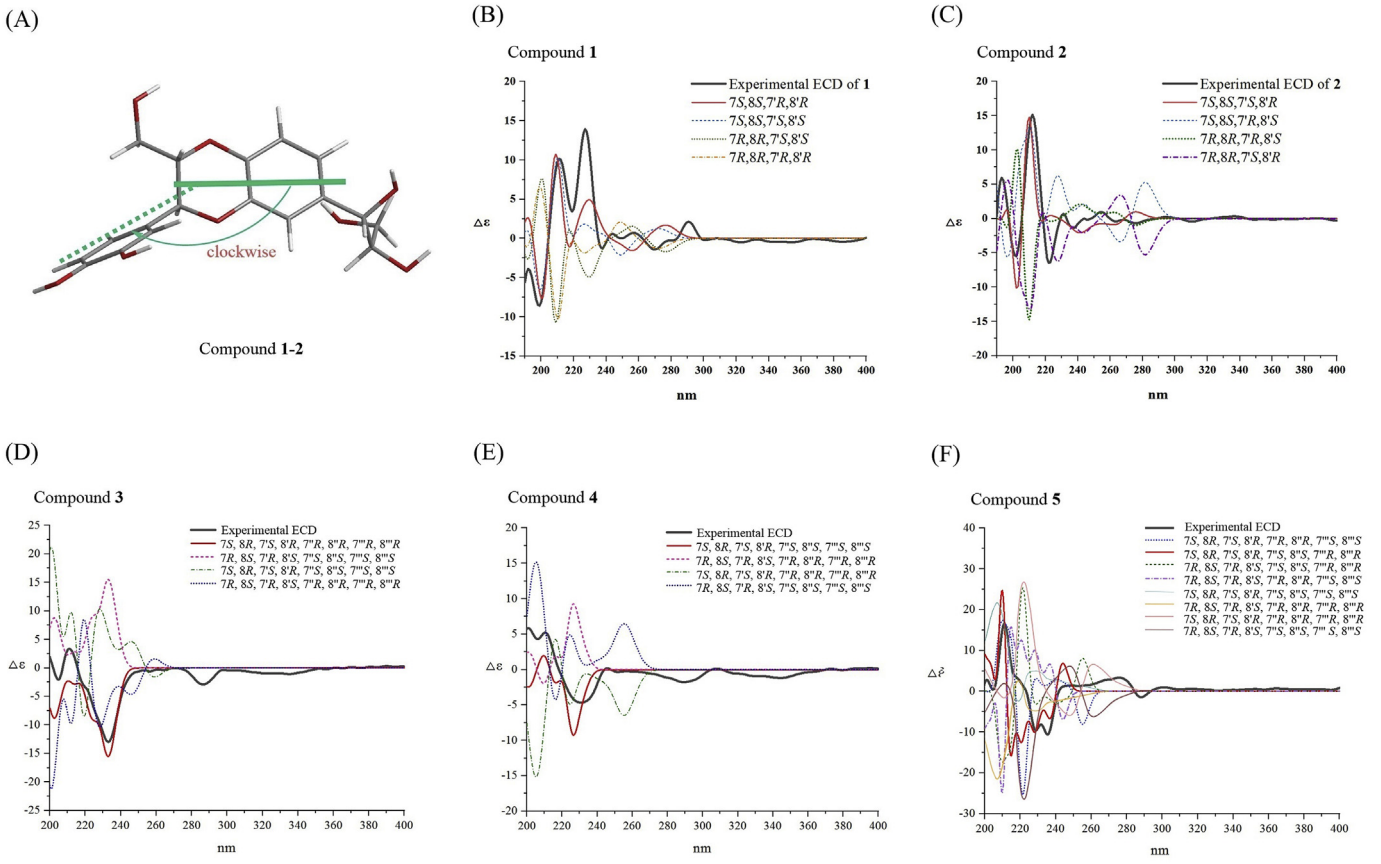

Fig. 4. (A) The CD exciton chirality model for **1** and **2**; (B)–(F) The calculated ECD spectra of **1** (B), **2** (C), **3** (D), **4** (E), and **5** (F).

Table 2
The ^{1}H-NMR (600 Hz) and^{13}C-NMR (150 Hz) data of compounds **3** and **4** (DMSO-d_6).

No.	Comp.**3**		Comp.**4**	
	δ_H	δ_C	δ_H	δ_C
1, 1′	–	134.5	–	134.7
2, 2′	6.88 (d, 1.7)	114.5 114.6	6.92 (d, 1.3)	114.4
3, 3′	–	143.4	–	143.0 143.1
4, 4′	–	142.6	–	142.9
5, 5′	6.89 (d, 8.3)	116.5	6.86 (d, 8.3)	116.6
6, 6′	6.85 (dd, 8.3, 1.7)	118.9 119.0	6.83 (dd,8.3,1.3)	118.8
7, 7′	4.62 (d, 3.3)	84.6	4.65 (d, 3.3)	84.6
8, 8′	3.0 (m)	53.6 53.7	3.01 (m)	53.7
9, 9′	4.11 (m) 3.75 (dd, 8.3, 3.1)	71.0	4.13 (dd,6,6,8.9) 3.77 (dd,3.2,9.1)	71.0
1″, 1‴	–	127.6	–	127.6
2″, 2‴	6.80 (br.s)	114.9	6.79 (br. s)	114.9
3″, 3‴	–	145.2	–	145.3
4″, 4‴	–	145.8	–	145.8
5″, 5‴	6.76 (d, 8.0)	115.5	6.75 (d, 7.6)	115.5
6″, 6‴	6.70 (dd, 8.0, 1.4)	118.8	6.68 (dd,7.6,1.0)	118.7
7″, 7‴	4.81 (d, 7.7)	75.7	4.80 (d, 7.7)	75.6
8″, 8‴	4.01 (m)	78.2	4.02 (m)	78.2
9″, 9‴	3.30 (dd,12.5,4.6) 3.52 (dd,12.4,2.2)	60.2	3.33 (dd,11.9,4.5) 3.51 (br.d, 12.0)	60.2

chemical shifts between **5** and **3**/**4** was mainly observed at the two additional caffeoyl alcohol segments with 3, 3′-bisdemethylpinoresinol. In HMBC, we observed the correlations from H-7″ to C-3 and from H-7‴ to C-4' (see Fig. 3), which led to the determination of the planar

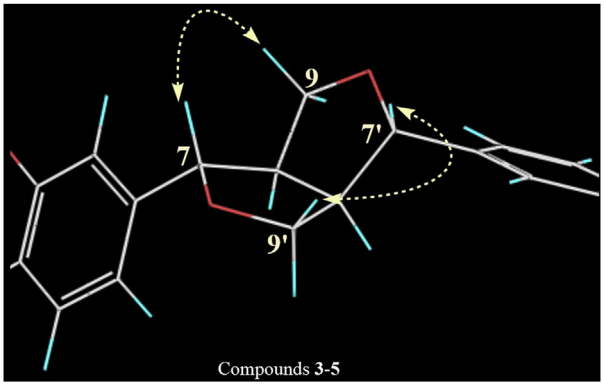

Fig. 5. Key NOE correlations of **3**–**5.**

structure possessing two monolignan fragments that existed in the structures of **3** and **4**, respectively, and thereby explained the reason for the absence of symmetric structures in **5**.

Proton signals at δ_H 4.79 (1H, d, J = 7.7 Hz, H-7″), 4.80 (1H, d, J = 7.7 Hz, H-7‴) indicated that both 7"/8″ and 7‴/8‴ existed as *trans* configurations, respectively. The 7-H/8-H *trans* and 7′-H/8′-H *trans* configurations were determined on the basis of values of $\Delta\delta_{H\text{-}9}$ and $\Delta\delta_{H\text{-}9'}$ ($\Delta\delta$ = 0.35) (Shao et al., 2018). The relative configurations of the H-7 and H-7′ of the furofuran ring system were confirmed by both the chemical shifts (Kamiya et al., 2004) and NOE correlations of H-7/H-9 and H-7'/H-9' (Fig. 5). The ECD calculation results showed that the cotton effects of 7*S*, 8*R*, 7′*S*, 8′*R*, 7″*S*, 8″*S*, 7*R*, 8*R* -isomer of **5** were in good agreement with those of the experimental CD spectra (Fig. 4F). Therefore, **5** was established as 7*S*, 8*R*, 7′*S*, 8′*R*, 7″*S*, 8″*S*, 7*R*, 8*R* -Di-verniciasin B.

Table 3
The ^{1}H-NMR (600 Hz) and^{13}C-NMR (150 Hz) data of compound **5** (DMSO-d_6).

No.	δ_H	δ_C	No.	δ_H	δ_C
1	–	134.5	1″	–	127.6
2	6.88 (d, 1.8)	114.5	2″	6.79 (d, 1.8)	115.0
3	–	143.4	3″,	–	145.3
4	–	142.6	4″	–	145.8
5	6.89 (d, 8.3)	116.5	5″	6.74 (d, 8.0)	115.5
6	6.85(dd, 8.3,1.8)	119.0	6″	6.69 (dd, 8.0, 1.8)	118.8
7	4.63 (d, 4.7)	84.6	7″	4.79 (d, 7.7)	75.7
8	3.0 (m)	53.7	8″	4.01 (m)	78.2
9	4.11 (dd, 8.8, 6.7) 3.76 (ddd, 9.1, 3.5, 1.9)	71.0	9″	3.32(dd, 12.1, 4.3) 3.51(dd, 12.1, 2.2)	60.2
1′	–	134.7	1‴	–	127.6
2′	6.91 (d, 1.8)	114.4	2‴	6.80 (d, 1.8)	115.0
3′	–	143.0	3‴	–	145.3
4′	–	142.9	4‴	–	145.8
5′	6.85 (d, 8.3)	116.6	5‴	6.75 (d, 8.0)	115.5
6′	6.82(dd, 8.3,1.8)	118.8	6‴	6.68 (dd, 8.0, 1.8)	118.7
7′	4.64 (d, 4.6)	84.6	7‴	4.80 (d, 7.7)	75.6
8′	3.0 (m)	53.7	8‴	4.01 (m)	78.2
9′	4.11 (dd, 8.8, 6.7) 3.76 (ddd, 9.1, 3.5, 1.9)	71.1	9‴	3.32(dd,12.3, 4.8) 3.51(dd, 12.1, 2.2)	60.2

Table 4
The ^{1}H-NMR (600 Hz) and^{13}C-NMR (150 Hz) data of compounds **6–8** (CD_3OD).

No.	Comp.**6**		Comp.**7**		Comp.**8**	
	δ_H	δ_C	δ_H	δ_C	δ_H	δ_C
1	–	131.4	–	131.4	–	131.4
2	6.77 (d, 1.9)	115.4	6.77 (d, 1.9)	115.4	6.80 (d, 1.9)	115.8
3	–	146.3	–	146.3	–	146.1
4	–	146.5	–	146.5	–	146.3
5	6.76 (d, 8.2)	116.2	6.76 (d, 8.0)	116.2	6.76 (d, 8.0)	116.0
6	6.65 (dd, 8.2, 1.9)	120.4	6.65 (dd, 8.0, 1.9)	120.4	6.67 (dd, 8.0, 1.9)	120.8
7	4.00 (d, 7.2)	85.6	3.99 (d, 7.2)	85.6	4.03 (d, 6.2)	85.7
8	3.65 (m)	77.1	3.66 (m)	77.1	3.70 (m)	76.3
9	3.40 (dd, 11.4, 3.5) 3.28 (dd, 11.4, 6.3)	63.9	3.40 (dd, 11.4, 3.5) 3.27 (dd, 11.4, 6.4)	63.9	3.66 (dd, 11.2, 3.6) 3.56 (dd, 11.2, 6.5)	64.3
-OCH_3	3.21 (s)	56.7	3.21 (s)	56.7	3.20 (s)	56.9

Compounds **6** and **7** were separated via a chiral separation as yellow syrup. Having opposite optical rotation values ([α]20D + 64.3 for **6** and [α] 20D - 87.9 for **7**), the ^{1}H and ^{13}C NMR spectra of **6** and **7** were identical to each other (Table 4), suggesting a pair of enantiomers. The chemical formulas of **6** and **7** were deduced by the positive HRESIMS *m/z* 237.0757 $[M+Na]^+$ (calcd. 237.0733 for $C_{10}H_{14}O_5Na$). In the ^{1}H NMR spectra, there were three aromatic proton signals presented in the low field as δ_H 6.77 (1H, d, J = 1.9 Hz, H-2), 6.76 (1H, d, J = 8.2 Hz, H-5), and 6.65 (1H, dd, J = 8.2, 1.9 Hz, H-6). In the high field, the signal at δ_H 3.21 (3H, s) was assigned to a methoxyl group. The coupling constant of H-7 at δ_H 4.00 (1H, d, J = 7.2 Hz) indicated that the relative configuration of C-7/C-8 was *threo* in both compounds **6** and **7** (Kim et al., 2013), suggesting that the absolute configurations for **6** and **7** were either 7*R*, 8*R* or 7*S*,8*S*. In the ^{13}C NMR spectra, six aromatic carbons (δ_C 146.5, 146.3, 131.4, 120.4, 116.2, 115.4), a secondary carbon (δ_C 63.9), two tertiary carbons (δ_C 85.6, 77.1) and a methoxyl group (δ_C 56.7) were revealed. The planar structures of **6** and **7** were finally established by HMBC correlations in Fig. 2. The methoxyl group was located at C-7 on the basis of the HMBC correlation from δ_H 3.21 (7-OCH_3) to δ_C 85.6 (C-7) (Fig. 3).

The absolute configurations of C-7 and C-8 were determined by comparing values of optical rotation with those of alatusols A-E in the literature (Kim et al., 2013). As a result, **6** with [α] 20D+ 64.3 was deduced to possess the 7*S*, 8*S*-configuration, while 7 with [α] 20D- 87.9 was elucidated to have the 7*R*, 8*R*-configuration. In order to further confirm the deduced absolute configurations of C-7 and C-8, the ECD calculation was performed. As **6** and **7** gave opposite cotton effects in their experimental ECD spectra (Fig. 6A), the 7*R*, 8*R* and 7*S*, 8*S* isomers were subjected to the ECD calculation. The results showed that cotton effects in the calculated ECD of the 7*R*,8*R*-isomer perfectly matched those in the experimental ECD spectra of **7** (Fig. 6B) while calculated ECD curves of the 7*S*,8*S*-isomer aligned perfectly with those of the experimental ECD spectra of **6**. Therefore, **6** and **7** were named as 7*S*, 8*S* -verniciasin D and 7*R*, 8*R* -verniciasin D, respectively.

The molecular formula of compound **8** was established as $C_{10}H_{14}O_5$ by the positive quasi-molecular ion peak in the HRESIMS *m/z* 237.0742 [M + Na] + (calcd. 237.0733 for $C_{10}H_{14}O_5Na$). All the spectroscopic data of **8** were similar to those of **6** and **7**, including a methoxyl group, a methylene group, two methine moieties and a set of ABX coupling system (Table 4). HMBC correlations (Fig. 3) revealed the same planar structure as that of **6** and **7**, indicating that **8** was an epimer of **6** and **7**. The coupling constant for H-7 of **8** was 6.2 Hz, which was smaller than that of **6** and **7** (Kim et al., 2013), further confirming that **8** was an epimer of **6** and **7**. All these aforementioned data suggested that the absolute configurations of **8** were either 7*S*, 8*R* or 7*R*,8*S*. Finally, the results of the ECD calculation (Fig. 6C) suggested that the absolute configurations of **8** were 7*R*,8*S*. Therefore, **8** was elucidated as 7*R*, 8*S*-verniciasin D.

The structures of the known compounds (Fig. 2) were elucidated to be isoprincepin (**9**) (Waibel et al., 2003), princepin (**10**) (Waibel et al., 2003), 3, 3′-bisdemethylpinoresinol (**11**) (Li et al., 2010), (+)-7-epi-sesamin-dicatechol (**12**) (Li et al., 2010), isoamericanol A (**13**) (Kim et al., 2010), 9′-methoxylisoamericanol A (**14**) (Zhao and Shen, 2004), isoamericanin A (**15**) (Kohei et al., 2004), americanin B (**16**) (Yu et al., 2001), 7*S*, 8*R*-americanin D (**17**) (Yang et al., 2009), 4-hydroxyl cinnamic aldehyde (**18**) (Luo and Zhang, 2011), 3, 4-dihydroxyl cinnamic aldehyde (**19**) (Li et al., 2014a, 2014b), 3- hydroxyl-4-methoxyl

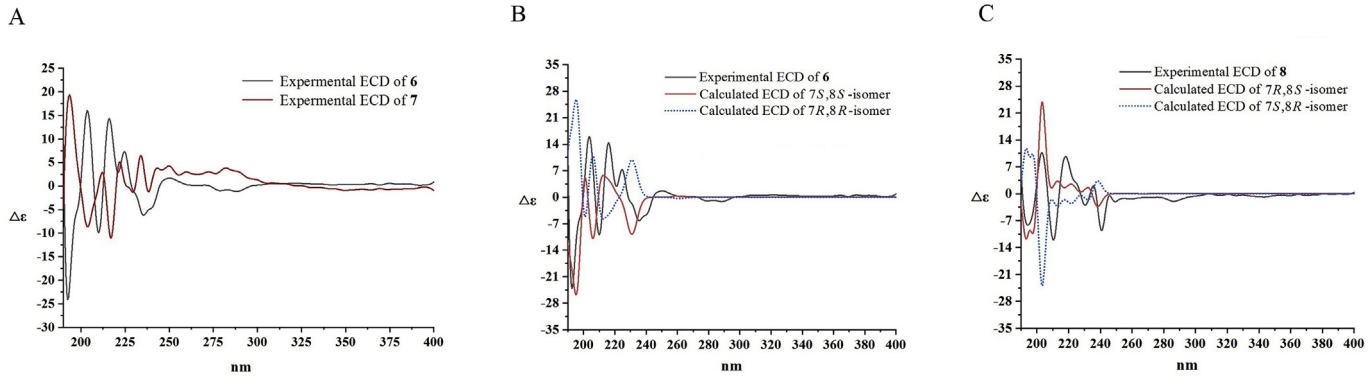

Fig. 6. (A) The experimental ECD spectra of **6** and **7**; (B) The experimental and calculated ECD spectra of **6**; (C) The experimental and calculated ECD spectra of **8**.

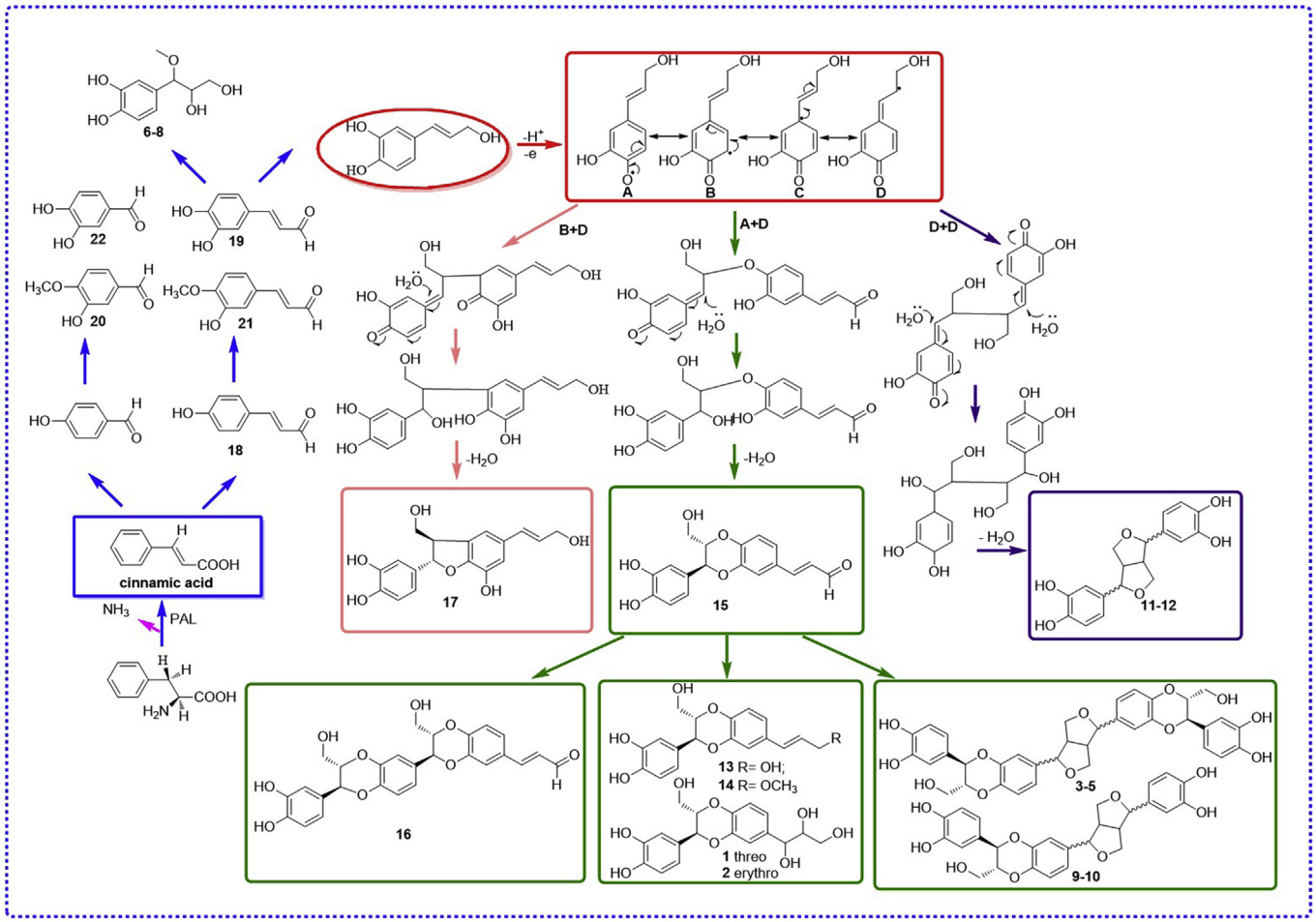

Fig. 7. Plausible biosynthesis pathways of the identified lignans **1**–**22**.

benzaldehyde (**20**) (Xu and Tan, 2012), 3-hydroxyl-4-methoxyl cinnamic aldehyde (**21**) (Zhu et al., 2012), 3, 4-dihydroxyl benzaldehyde (**22**) (Lu et al., 2014), and 24*R*-6*β*-hydroxy-24-ethylcholest-4-en-3-one (**23**) (Yoko et al., 1998).

Based on the characteristics of the identified structures, a plausible biosynthetic pathway was proposed as shown in Fig. 7. The biosynthetic precursor of lignans could be admitted to cinnamic acid, which was obtained when phenylalanine deaminized (Ma et al., 2011; Markulin et al., 2019; Satake et al., 2015; Yang et al., 2017). Eight phenylpropanoids **6**–**8** and **18**–**22** came from the starting compound-cinnamic acid by reactions of reduction, methylation, and hydroxylation (Satake et al., 2013). Through a series of redox reactions, cinnamic acid was also converted to demethylconiferol, which could form four types of resonances (A-D) via a deionization reaction. Afterwards, two resonances (B and D) could construct monolignan **17** via electrophilic addition and dehydration condensation. Similarly, monolignans **1**–**2**, **13**–**15** were derived from the condensation and oxygenation of units A and D. Additionally, the key intermediate **15** could further yield three dineolignans **3**–**5** and three sesquineolignans **9**–**10**, **16** via cyclization. In addition, other monolignans **11**–**12** may result from two D moieties through addition and dehydration reactions.

2.2. Anti-neuroinflammatory effects of isolated components from V. fordii

The extracts and identified components (**1**–**23**) were evaluated *in vitro* for their anti-neuroinflammatory activities in LPS-induced BV2 cells and the results are displayed in Table 5 and Fig. 8. In order to avoid a false positive result, cell toxicities of the tested samples (supporting information Table S1) were assayed via MTT methods in normal BV2 cells. The 70% ethanol extract of the seed testa of *V. fordii* significantly inhibited the production of NO in LPS-activated BV2 cells with an IC_{50} value of 7.03 μg/mL. Further assays indicated that the ethyl acetate extract (69.38%) with an IC_{50} value of 10.70 μg/mL from the crude extract might be the bioactive fraction of the herbal.

Subsequently, components identified from the EtOAc extract were

Table 5
Effects of extracts and compounds isolated from *Vernicia fordill* on NO production in LPS-activated BV2 microglia cells.

No.	IC_{50} (μM)	No.	IC_{50} (μM)
YTK[a]	7.03 ± 0.92	Comp. 11	18.47 ± 1.38
YTK-1[a]	22.05 ± 1.77	Comp. 12	16.93 ± 1.62
YTK-2[a]	10.70 ± 1.36	Comp. 13	66.84 ± 2.56
YTK-3[a]	44.12 ± 1.80	Comp. 14	38.82 ± 1.97
Comp. 1	> 100	Comp. 15	9.88 ± 2.38
Comp. 2	> 100	Comp. 16	6.82 ± 2.13
Comp. 3	11.49 ± 3.67	Comp. 17	12.66 ± 2.25
Comp. 4	5.86 ± 2.59	Comp. 18	2.18 ± 1.61
Comp. 5	2.91 ± 1.51	Comp. 19	> 100
Comp. 6	> 100	Comp. 20	75.87 ± 2.83
Comp. 7	> 100	Comp. 21	2.39 ± 1.58
Comp. 8	> 100	Comp. 22	45.80 ± 2.23
Comp. 9	1.28 ± 1.09	Comp. 23	2.60 ± 1.62
Comp. 10	9.80 ± 1.42	Mino	37.04 ± 2.09

YTK: 70% ethanol crude extract; YTK-1: petroleum ether extract; YTK-2: ethyl acetate extract; YTK-3: *n*-butanol extract; Mino: minocycline; [a] the concentration for the extracts was μg/mL.

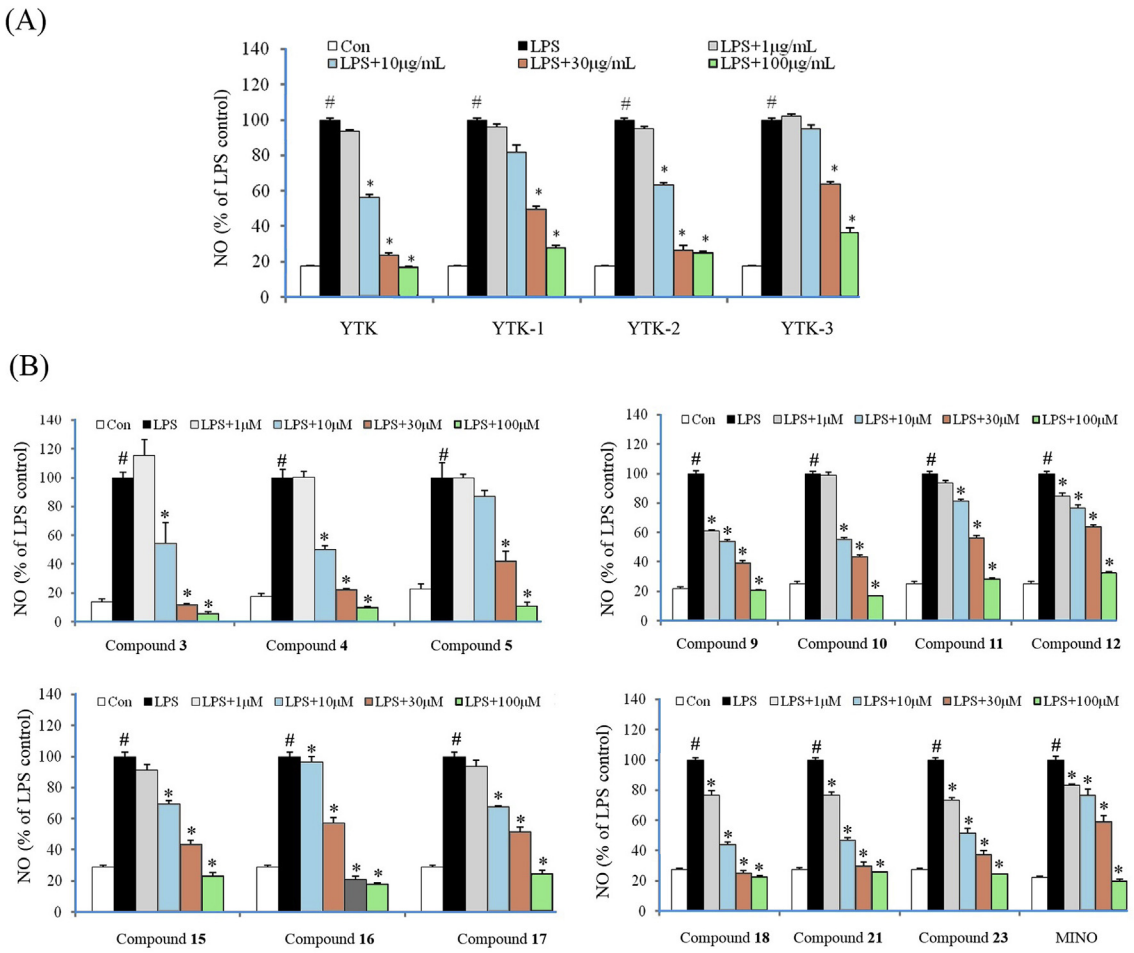

Fig. 8. Effects of the extracts and bioactive compounds **3–5**, **9–12**, **15–17**, **18**, **21** and **23** on LPS-induced NO production in microglial cells. (A) Inhibitory effects of the extracts. (B) Inhibitory effects of the identified compounds **3–5**, **9–12**, **15–17**, **18**, **21** and **23**. (BV-2 cells were treated with tested samples in the presence of LPS (100 ng/mL) for 24 h. NO production was tested by Griess reaction. Data are expressed as means ± SEM (n = 3). $^{\#}P < 0.05$ compared with the control group, $^{*}P < 0.05$ compared with LPS group. YTK: 70% ethanol crude extract; YTK-1: petroleum ether extract; YTK-2: ethyl acetate extract; YTK-3: *n*-butanol extract; Mino: minocycline using as positive control).

evaluated for their anti-neuroinflammatory activities. As a result, 13 lignans showed more potent inhibitory effects with IC_{50} values from 1.28 to 18.47 μM than the positive control (minocycline, IC_{50} = 37.04 μM). The effective ingredients were structurally characterized as dineolignans (compounds **3**, **4**, **5**), sesquineolignans (compounds **9**, **10**, **16**), monolignans (compounds **11**, **12**, **15**, **17**), and phenylpropanoids (compounds **18**, **21**, **23**). Additionally, compounds **13**, **14**, **20**, **22** elicited moderate anti-neuroinflammatory activities with IC_{50} values ranging from 38.82 to 75.87 μM.

On the basis of the above-mentioned results, brief structure and activity relationships could be concluded as follows: firstly, the presence of 1, 4-bendioxanes enhanced the inhibitory effect against NO production, such as compounds **9** vs **11**, **10** vs **12**, and **15** vs **16**.

Second, compound **13** substituted by a hydroxyl group at C-9′ exhibited moderate inhibitory activity while compound **14** with a methoxyl group at C-9′ displayed a significant inhibitory effect (Table 5), indicating that the 9′-OMe enhanced the inhibitory activity of isoamericanol A.

In addition, for phenylpropanoids, such as compounds **18–22**, both the reduction of C-3 hydroxyl or methoxylation of C-4 hydroxyl can increase inhibitory activities, such as compounds **18** vs **19** and **20** vs **22**.

*2.3. Effects of compounds **9**, **10**, **16** and **18** on LPS-induced overexpression of inflammatory mediators*

Taking the inhibitory effects and amounts of the identified compounds **1–23**, four principle bioactive components (**9**, **10**, **16**, and **18**) were further investigated for the action mechanisms. Their effects on LPS-induced TNF-α, IL-1β and IL-6 overexpression in microglial cells were tested via the qRT-PCR method. The result revealed that compounds **9**, **10**, **16**, and **18** significantly inhibited LPS-induced TNF-α, IL-1β and IL-6 production at 10 μM as shown in Fig. 9.

3. Conclusion

Chronic neuroinflammation induced by over-activated microglia is considered to be a critical cause of the neurodegenerative disease. However, nonsteroidal anti-inflammatory drugs (NSAIDs) and estrogen, the most commonly used clinical drugs for neuroinflammation, can trigger severe side effects for patients with long-term medication. Therefore, effective natural neuroinflammatory inhibitors with low side effects can throw light on the development of therapy for neurodegenerative disease.

In this paper, a series of previous undescribed bioactive components (**1–8**), along with 15 known ones, from *V. fordii* were reported in this paper. The lignans from *V. fordii* were mainly composed of two types of substructures, benzodioxane and bistetrahydrofuran. The dineolignans

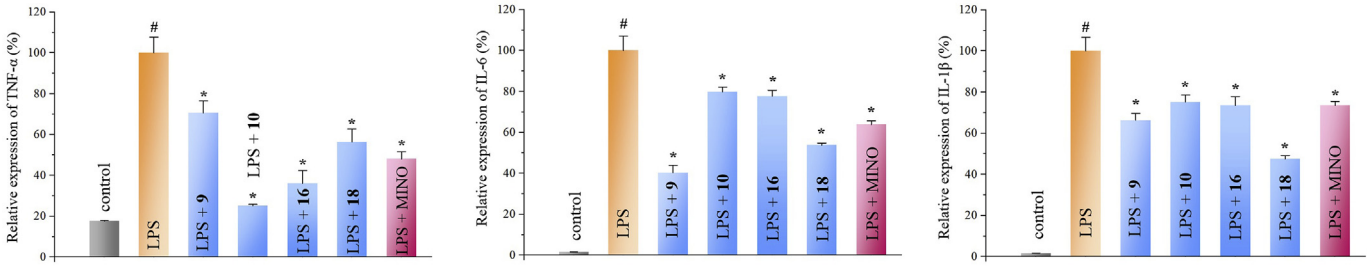

Fig. 9. Effects of the bioactive components (**9**, **10**, **16**, and **18**) on LPS-induced TNF-α, IL-1β and IL-6 overexpression in microglial cells. BV-2 microglial cells were pretreated with tested compounds (10 μM) for 2 h and then stimulated with LPS (100 ng/mL) for 24 h. Total RNA was isolated 4 h after LPS treatment and the mRNA levels of TNF-α, IL-1β and IL-6 were measured by qRT-PCR. Data are expressed as means ± SEM (n = 4). $^{\#}P < 0.001$ compared with the untreated cells (control group); $^{*}P < 0.05$ compared with the cells treated with LPS alone (LPS group).

(**3–5**) were composed of two 1, 4-benzodioxane units and one bistetrahydrofuran moiety; the sesquineolignans **9** and **10** were formed via one 1, 4-benzodioxane fragment and one bistetrahydrofuran unit; and compound **16** was comprised of two 1, 4-benzodioxane units.

The *in vitro* assay showed that most of these isolated components (**3–5**, **9–18**, and **20–23**) from *V. fordii* had anti-neuroinflammatory activities, suggesting that *V. fordii* has a great potential in the treatment of neuroinflammation.

4. Experimental

4.1. General

Optical rotations were performed on a PerkinElmer Model 341 polarimeter. CD spectra was measured on JASCO pu-2080.^{1}H-NMR and ^{13}C-NMR spectra were recorded on Bruker AV-400 NMR spectrometers with TMS as an internal standard, while 2D NMR spectra were recorded on Bruker AV-600 NMR spectrometers. HRESI-MS was measured on Bruker micro-TOFQ-Q mass spectrometer. Column chromatography (CC) was performed with Silica gel (Qingdao Marine Chemical Co. Ltd.). ODS (50 μm, YMC Co. Ltd., Kyoto, Japan); Sephadex LH-20 (Amersham Pharmacia Biotech AB; SE-715 84 Uppsala Sweden); Macroporous resin HPD-100 (Cangzhou Baoen Chemical Co. Ltd.); preparative HPLC was conducted on a YMC ODS column (5 μm, 20 mm × 250 mm) equipped with a Shimadzu LC-6AD pump and a RID-10A detector. Chiral HPLC separation was conducted on a Daicel IF column (5 μm, 0.46 cm × 25 cm) with a LC-10AD pump system (Shimadzu) and a UV detector (SPD-20A). Fetal bovine serum (FBS) and Dulbecco's Modified Eagle's Medium (DMEM) were from Tianjin haoyang Biological Manufactory Co., Ltd (Tianjin, China) and Gibco BRL (Grand Island, NY, USA), respectively.

4.2. Plant material

Testae prepared by removing seed kernel of *Vernicia fordii* (Hemsl.) Airy Shaw (Euphorbiaceae), which grown at the town of Hongjiang, were provided by Ningbolihua Plant Extraction Technology Co. Ltd. (Zhejiang, China) and identified by Prof. Yingni Pan, School of Traditional Chinese Materia Media, Shenyang Pharmaceutical University. The voucher specimen (20130913) was deposited in the Department of Natural Products Chemistry, Shenyang Pharmaceutical University, Shenyang, China.

4.3. Extraction and isolation

The air-dried testa of *V. fordii* (3.2 kg) was powdered and extracted under reflux with 70% EtOH (3 × 2h × 25 L). Then, the crude extract (320.0 g) was dissolved in 2 L hot water and participated with petroleum ether (PE), ethyl acetate (EtOAc), *n*-butyl alcohol (*n*-BuOH) respectively.

The EtOAc extract (222.0 g) was purified by silica column chromatography (110 × 10.5 cm) eluted with CH_2Cl_2/MeOH (100: 0–0:100) to afford five fractions (Fr 2.1-Fr 2.5). Compounds **13** (780 mg) and **14** (19 mg) were isolated from Fr 2.1 by recrystallization and Sephadex LH-20 column. Comp. **15** (2.0 g, PE/Actone, 100: 2, V/V) and Comp. **16** (23.5 mg, PE/Acetone, 100: 3, V/V) were purified by recrystallizing from Fr 2.1. Comp. **20** (2 mg, t_R = 60 min) and Comp. **21** (13 mg, t_R = 65 min) were isolated by first separated on silica gel column with gradient elution (PE/Acetone, 100:0–0:100) and then purified by HPLC (YMC, 250 × 10 mm, 5 μm, MeOH/H_2O, 10:90, V/V, 2 mL/min). Comp. **18** (14 mg, PE/Actone, 100: 2, V/V) and Comp. **23** (4.6 mg, PE/Acetone, 100: 4, V/V) were purified by recrystallizing from Fr 2.1. Fr. 2.2 was chromatographed on ODS column to afford four subfractions (Fr 2.2.1-Fr 2.2.4) with gradient elution (MeOH/H_2O, 10%, 30%, 50%, 70%). Comp. **22** (58 mg, t_R = 28 min) was isolated from Fr 2.2.1 by isocratic semi-preparative HPLC (MeOH/H_2O, 15: 85, V/V, 2 mL/min). While, Comp. **6** (4.1 mg), Comp. **7** (2.1 mg) and Comp. **8** (2.2 mg) were isolated as isomer from Fr 2.2.1 by chiral separation (Ph-CD, 250 × 10 mm, 5 μm, MeOH/H_2O, 5: 95) with MeOH/H_2O as elution solvent. Fr 2.2.2 was purified by HPLC (MeOH/H_2O, 25: 75, V/V, 2.5 mL/min) to obtain Comp. **19** (27 mg, t_R = 23 min) and Comp. **11** (30 mg, t_R = 31 min). Compound **17** (9 mg) was gained by recrystallizing from Fr 2.2.2. Fr 2.2.3 was subjected to RP-HPLC with MeCN/H_2O (30:70, V/V, 2 mL/min) to yield Comp. **9** (10 mg, t_R = 8 min). Besides, Fr 2.2.4 was submitted to HPLC (MeCN/H_2O, 30:70, V/V) on the RP-C18 column to produce Comp. **14** (20 mg, t_R = 16 min). Subsequently, using ODS column and LH-20, Fr 2.3 was fractioned two sections. The first section was separated on reversed phase HPLC (MeCN/H_2O, 30:70, V/V, 2 mL/min) to give Comp. **10** (14 mg, t_R = 17 min) and Comp. **12** (13 mg, t_R = 13 min), while, the second section was purified on preparative column to obtain 3 subfraction (1st, 26 mg, t_R = 26 min; 2nd, 32 mg, t_R = 34 min; 3rd, 21 mg, t_R = 43 min) with MeCN/H_2O (68:32, V/V, 6.5 mL/min) as elution solvent. After the chiral separated by HPLC eluting with *n*-hexane/ethanol (90:10, V/V, 1 mL/min), the 1st was further purified to comp. **3**, the 2nd one was purified to comp. **4**, and the 3rd one was purified to comp. **5**. Comp. **1** (17 mg, t_R = 35 min) and Comp. **2** (19 mg, t_R = 55 min) were isolated from Fr 2.5 by HPLC (MeOH/H_2O, V/V, 10:90, 6.5 mL/min).

4.4. 7, 8-trans-7′, 8′- threo-verniciasin B (1)

Yellow syrup (MeOH). UV(MeOH) λ_{max}: 215, 258 nm [α] 20D -13.6 (*c* 0.15, MeOH). IR(KBr) ν_{max} 3350, 3016, 2890, 2810, 1610, 1508, 1421, 1033, 920 cm^{-1}. The negative HRESI-MS (*m/z*): 363.1083 $[M-H]^-$ (calcd. 363.1085 for $C_{18}H_{20}O_8$). The data of ^{1}H-NMR (400 MHz, DMSO-d_6) and ^{13}C-NMR (100 MHz, DMSO-d_6) see Table 1.

4.5. 7, 8-trans-7′, 8′-erythro-verniciasin B (2)

Yellow syrup (MeOH). UV(MeOH) λ_{max}: 218, 255 nm [α] 20D-35.9 (*c* 0.15, MeOH). IR(KBr) ν_{max} 3355, 3012, 2881, 2815, 1610, 1511, 1431, 1041, 910 cm^{-1}. HRESI-MS (*m/z*): 363.1085 $[M-H]^-$ (calcd. 363.1085 for $C_{18}H_{20}O_8$). The data of ^{1}H-NMR (400 MHz, DMSO-d_6) and ^{13}C-NMR (100 MHz, DMSO-d_6) see Table 1.

4.6. Isodiverniciasin A (3)

Colorless amorphous solid (MeOH). UV(MeOH) λ_{max}: 215, 250 nm [α] 20D-10.0 (*c* 0.1, MeOH). IR(KBr) ν_{max} 3420, 3015, 2950, 2885, 2810, 1650, 1508, 1320, 1010, 885 cm^{-1}. HRESI-MS (*m/z*): 681.1942 $[M+Na]^+$ (calcd. 681.1940 for $C_{36}H_{34}NaO_{12}$). The data of ^{1}H-NMR (600 MHz, DMSO-d_6) and ^{13}C-NMR (150 MHz, DMSO-d_6) see Table 2.

4.7. Diverniciasin C (4)

Colorless amorphous solid (MeOH). UV(MeOH) λ_{max}: 212, 260 nm [α] 20D-61.0 (*c* 0.1, MeOH). IR(KBr) ν_{max} 3420, 3010, 2950, 2880, 2810, 1630, 1508, 1320, 1020, 885 cm^{-1}. HRESI-MS (*m/z*): 657.1974 $[M-H]^-$ (calcd. 657.1978 for $C_{36}H_{34}O_{12}$). The data of ^{1}H-NMR (600 MHz, DMSO-d_6) and ^{13}C-NMR (150 MHz, DMSO-d_6) see Table 2.

4.8. Diverniciasin B (5)

Colorless amorphous solid (MeOH). UV(MeOH) λ_{max}: 219, 258 nm [α] 20D -181.0 (*c* 0.1, MeOH). IR(KBr) ν_{max} 3410, 3015, 2950, 2880, 2810, 1660, 1501, 1320, 1031, 890 cm^{-1}. HRESI-MS (*m/z*): 657.1984 $[M-H]^-$ (calcd. 657.1978 for $C_{36}H_{34}O_{12}$). The data of ^{1}H-NMR (600 MHz, DMSO-d_6) and ^{13}C-NMR (150 MHz, DMSO-d_6) see Table 3.

4.9. 7S, 8S-verniciasin D (6)

Yellow syrup (MeOH). UV(MeOH) λ_{max}: 215, 251 nm [α] 20D + 64.3 (*c* 0.09, MeOH). IR(KBr) ν_{max} 3355, 3016, 2951, 2880, 2800, 1600, 1518, 1320, 1010, 890 cm^{-1}. HRESI-MS (*m/z*): 237.0757 $[M+Na]^+$ (calcd. 237.0733 for $C_{10}H_{14}O_5Na$). The data of ^{1}H-NMR (600 MHz, CD_3OD) and ^{13}C-NMR (150 MHz, CD_3OD) see Table 4.

4.10. 7R, 8R-verniciasin D (7)

Yellow syrup (MeOH). UV(MeOH) λ_{max}: 216, 252 nm [α] 20D -87.9 (c 0.05, MeOH). IR(KBr) ν_{max} 3360, 3011, 2950, 2885, 2800, 1620, 1519, 1310, 1025, 920 cm^{-1}. HRESI-MS (*m/z*): 237.0753 $[M+Na]^+$ (calcd. 237.0733 for $C_{10}H_{14}O_5Na$). The data of ^{1}H-NMR (600 MHz, CD_3OD) and ^{13}C-NMR (150 MHz, CD_3OD) see Table 4.

4.11. 7R, 8S-verniciasin D (8)

Yellow syrup (MeOH). UV(MeOH) λ_{max}: 216, 261 nm [α] 20D-17.9 (c 0.05, MeOH). IR(KBr) ν_{max} 3340, 3025, 2950, 2890, 2805, 1620, 1519, 1320, 1035, 925 cm^{-1}. HRESI-MS (*m/z*): 237.0742 $[M+Na]^+$ (calcd. 237.0733 for $C_{10}H_{14}O_5Na$). The data of ^{1}H-NMR (600 MHz, CD_3OD) and ^{13}C-NMR (150 MHz, CD_3OD) see Table 4.

4.12. Cell culture

The BV2 cell was afforded by Professor Yuanqiang Guo's lab, Nankai University. BV2 cells were grown at 37 °C in DMEM supplemented with 10% FBS, 100 μg/mL penicillin and 100 μg/mL streptomycin with 5% CO_2.

4.13. Determination of cell viability

Before conducting the anti-inflammatory activity test of the isolated compounds, we performed the cytotoxicity test first in BV2 cells. BV2 cells viability was tested by MTT method represented in previous work (Hou et al., 2015; Li et al., 2014a, 2014b, 2015a, 2015b). The cells were plated into 96-well plates and treated with tested compounds and LPS for 24 h. After the supernatant taken away, MTT (0.25 mg/mL) was added into the plate, then incubated for 4 h at 37 °C. At last, the formazan crystals would be dissolved in DMSO and the absorbance of each well would be recorded at 490 nm by using a plate reader (Bio-Tek, Winooski, VT, USA).

4.14. Nitrite assay

The production of NO in LPS-induced BV2 cells was tested by Griess reaction (Hou et al., 2015; Li et al., 2014a, 2014b, 2015a, 2015b). The cells were plated into 96-well plates and incubated with tested sample with 100 ng/mL LPS. 24 h later, Griess reagent was added into the supernatant at room temperature. And the plate was read on a plate reader at 540 nm after 15 min.

4.15. Quantitative real-time PCR (qRT–PCR)

The total RNA was extracted with Trizol according to the manufacturer's instructions and converted to cDNAs. For quantitative RT-PCR, total RNA (2 μg) was reversely transcribed with reverse transcription-primers (Table S2) and Moloney murine leukaemia virus reverse transcriptase (Promega, Madison, WI, USA). Quantitative PCR reactions were done with Platinum SYBR Green qPCR SuperMix-UDG reagents (Invitrogen, Carlsbad, CA, USA) and Bulge-Loop primers (RiboBio) on the PRISM 7900HT system (Applied Biosystems, Carlsbad, CA, USA) with GAPDH as the normalisation control.

4.16. ECD calculation

All structures were established by Schrodinger 2013) package. Conformational searches were performed using the bioactive search function of conformational search protocol of the Schrodinger 2013 package with maximum 50 conformers. The conformers generated from conformational search were optimized at the B3LYP/6-31G (d) level using Gaussian 09 package. The optimized conformers were aligned using the flexible ligand alignment protocol to examine if there were identical conformers for some structurally similar conformers would lead to the totally identical conformer after structure optimization. After merging the identical conformers, the remaining conformers were subjected to frequent analysis at the B3LYP/6-31G (d) level. Then all the conformers were subject to DFT calculation at the B3LYP/6-31G (d) level using gaussian09 to generate ECD data of each conformer. Then the obtained ECD data were Boltzmann averaged to give the final ECD spectra.

Acknowledgments

The work was supported partially by National Natural Science Foundation of China (Grant No. 81673323, 81872768 , U1903122 , 81628012, U1603125), LiaoNing Revitalization Talents Program (XLYC1807118), Liaoning BaiQianWan Talents Program (2018), State Key Laboratory for Chemistry and Molecular Engineering of Medicinal Resources (Guangxi Normal University, CMEMR2018-B01) and the Fundamental Research Funds for the Central Universities of China (N182008004, N182006001).

Appendix A. Supplementary data

Supplementary data to this article can be found online at https://doi.org/10.1016/j.phytochem.2019.112233.

References

Adam, W., Lukacs, Z., Viebach, K., Humpf, H.U., Saha-Moller, C.R., Schreier, P., 2000. Microscale determination of the absolute configuration of alpha-aryl-substituted alcohols by the CD exciton chirality method. J. Org. Chem. 65, 186–190.

Gan, M.L., Zhang, Y.L., Lin, S., Liu, M.T., Song, W.X., Zi, J.C., Yang, Y.C., Fan, X.N., Shi, J.G., Hu, J.F., Sun, J.D., Chen, N.H., 2008. Glycosides from the root of iodes cirrhosa. J. Nat. Prod. 71, 647–654.

Guo, S.N., Guo, Z.Y., Ran, T.T., 2002. Basilicon for Treating Burn, Wound and Cold Injury, and its Preparation Method. Faming Zhuanli Shenqing CN 1357369 A 20020710.

Hirota, M., Ohigashi, H., Koshimizu, K., 1979. Piscicidal constituents and related diterpene esters from Aleurites fordii. Agric. Biol. Chem. 43, 2523–2529.

Hou, Y., Li, N., Xie, G., Wang, J., Yuan, Q., Jia, C., Liu, X., Li, G., Tang, Y., Wang, B., 2015. Pterostilbene exerts anti-neuroinflammatory effect on lipopolysaccharide-ctivated microglia via inhibition of MAPK signaling pathways. J. Funct. Foods 19, 676–687.

Kamiya, K., Tanaka, Y., Endang, H., Umar, M., Satake, T., 2004. Chemical constituents of Morinda citrifolia fruits inhibit copper-induced low-density lipoprotein oxidation. J. Agric. Food Chem. 52, 5843–5848.

Kim, K.H., Moon, E., Kim, S.Y., Lee, K.R., 2010. Lignans from the tuber-barks of *Colocasia antiquorum var.* esculenta and their antimelanogenic activity. J. Agric. Food Chem. 58, 4779–4785.

Kim, K.H., Ha, S.K., Choi, S.U., Kim, S.Y., Lee, K.R., 2013. Phenolic constituents from the twigs of *Euonymus alatus* and their cytotoxic and anti-inflammatory activity. Planta Med. 79, 361–364.

Kohei, K., Yohei, T., Hanani, E., Mansur, U., Toshiko, S., 2004. Chemical Constituents of *Morinda citrifolia* fruits inhibit copper-induced low-density lipoprotein oxidation. J. Agric. Food Chem. 52, 5843–5848.

Li, L., Li, X.F., Wu, H.X., 2010. Chemical constituents of anti oxidative activities from seeds of *Jatropha curcas*. Chin. Tradit. Herb. Drugs 41, 1932–1936.

Li, N., Ma, Z.J., Li, M.J., Xing, Y.C., Hou, Y., 2014a. Natural potential therapeutic agents of neurodegenerative diseases from the traditional herbal medicine Chinese dragon's blood. J. Ethnopharmacol. 152, 508–521.

Li, W., Tian, X.Y., Xiao, C.J., Jiang, B., 2014b. Chemical constituents from the underground parts of *Isodon phyllostachys*. Chin. Pharmaceut. J. 49, 1382–1385.

Li, J.Y., Jiang, Z., Li, X.Z., Hou, Y., Liu, F., Li, N., Liu, X., Yang, L.H., Chen, G., 2015a. Natural therapeutic agents for neurodegenerative diseases from a traditional herbal medicine *Pongamia pinnata* (L.) Pierre. Bioorg. Med. Chem. Lett 25, 53–58.

Li, N., Meng, D.L., Pan, Y., Cui, Q.L., Li, G.X., Ni, H., Sun, Y., Qing, D.G., Jia, X.G., Pan, Y.N., Hou, Y., 2015b. Anti-neuroinflammatory and NQO1 inducing activity of natural phytochemicals from *Coreopsis tinctoria*. J. Funct. Foods 17, 837–846.

Liao, B.Y., 2009. A Topical Drug for the Treatment of Burn and Scald. Faming zhuanli shenqing CN 101342224 A 20090114.

Lu, H.X., Li, J.Z., Nong, X.Z., Fu, Y.X., 2014. Chemical constituents of ethyl acetate extract from *Stenoloma chusanum*. Chin. J. Exp. Tradit. Med. Formul. 20, 114–117.

Luo, C., Zhang, W.N., 2011. Chemical constituents of *Opuntia milpa* alta haw (I). Chin. Tradit. Herb. Drugs 42 (3), 437–439.

Ma, S.G., Tang, W.A., Liu, Y.X., Hu, Y.C., Yu, S.S., Zhang, Y., Chen, X.G., Qu, J., Ren, J.H., Liu, Y.B., Xu, S., Liu, J., Liu, Y.Y., Li, Y., Lu, H.N., Wu, X.F., 2011. Prenylated C_6-C_3 compounds with molecular diversity from the roots of *Illicium oligandrum*. Phytochemistry 72, 115–125.

Mao, S. M., Zhang, H. Y., Zhang, S., Liu, Z. H. J. N. P. R, Development, 2012. Chem. Constituents of the Seeds of Vernicia fordii. 24, 1557-1560.

Markulin, L., Corbin, C., Renouard, S., Drouet, S., Gutierrez, L., Mateljak, I., Auguin, D., Hano, C., Fuss, E., Laine, E., 2019. Pinoresinol-lariciresinol reductases, key to the lignan synthesis in plants. Planta 249, 1695–1714.

Okuda, T., Yoshida, T., Koike, S., Toh, N., 1975. New diterpene esters from Aleurites fordii fruits. Phytochemistry 14, 509–515.

Pei, Y.H., Kwon, O.K., Lee, J.S., Cha, H.J., Ahn, K.S., Oh, S.R., Lee, H.K., Chin, Y.W., 2013. Triterpenes with cytotoxicity from the leaves of Vernicia fordii. Chem Pharm Bull (Tokyo) 61, 674–677.

Ran, Q.J., 2009. A Chinese Medicinal Composition for the Treatment of Burn and Scald. Faming Zhuanli Shenqing CN 101596258 A 20091209.

Reiner, W., Gerd, B., Monika, B., Hans, A., 2003. Sesquineolignans and other constituents from the seeds of *Joannesia princeps*. Phytochemistry 62, 805–811.

Satake, H., Ono, E., Murata, J., 2013. Recent advances in the metabolic engineering of lignan biosynthesis pathways for the production of transgenic plant-based foods and supplements. J. Agric. Food Chem. 61, 11721–11729.

Satake, H., Koyama, T., Bahabadi, S.E., Matsumoto, E., Ono, E., Murata, J., 2015. Essences in metabolic engineering of lignan biosynthesis. Metabolites 5, 270–290.

Shao, S.Y., Yang, Y.N., Feng, Z.M., Jiang, J.S., Zhang, P.C., 2018. An efficient method for determining the relative configuration of furofuran lignans by ^{1}H NMR spectroscopy. J. Nat. Prod. 81, 1023–1028.

Waibel, R., Benirschke, G., Benirschke, M., Achenbach, H., 2003. Sesquineolignans and other constituents from the seeds of Joannesia princeps. Phytochemistry 62, 805–811.

Xie, Y.F., Tao, Z.M., Wang, H.B., Qin, G.W., 2010. Chemical constituents from the roots of *Vernicia fordii*. 8, 264–266.

Xu, J.J., Tan, N.H., 2012. Phenolic compounds from *Jatropha curcas*. J. Chin. Mater. Med. 37, 3074–3077.

Yang, X.L., Jiang, M.Y., Hsieh, K.L., Liu, J.K., 2009. Chemical constituents from the seeds of *Morinda citrifolia*. Chin. J. Nat. Med. Mar. 7, 119–122.

Yang, X.Y., Zhang, Y.F., Liu, L.J., Wang, Y., Shang, M.Y., Xu, F., Liu, G.X., Cai, S.Q., 2017. Lignans and diterpenes isolated from *Tirpitzia ovoidea* and their biological activities. Chin. J. Nat. Med. 15 (12), 938–943.

Yoko, A., Tomomi, N., Mari, H., Kenji, S., Hiroyuki, A., Osama Basher, A.H., 1998. Chemical constituents of aquatic fern *Azolla Nilotica*. Phytochemistry 4, 471–474.

Yu, J.G., Li, T.M., Sun, L., Luo, X.Z., Ding, W., Li, D.Y., 2001. Studies on the chemical constituents of the seeds from *artabostrys hexapets* alues (annonaceae). Acta Pharm. Sin. 36, 281–286.

Zhang, G.H., 2003. A Topical Medicine Comprises Chinese Herbs for the Treatment of Burn and Scald. Faming Zhuanli Shenqing CN 1411825 A 20030423.

Zhao, P.J., Shen, Y.M., 2004. Neo-lignans in the seed crusts of *Trewia nudiflora*. Chin. Chem. Lett. 15, 921–924.

Zhu, J.X., Ren, J., Qin, J.J., Cheng, X.R., Zeng, Q., Zhang, F., Yan, S.K., Jin, H.Z., Zhang, W.D., 2012. Phenylpropanoids and lignanoids from euonymus acanthocarpus. Arch Pharm. Res. (Seoul) 35, 1739–1747.